FULL PAPER

Multicomponent Self-Assembly with a Shape Persistent *N*-Heterotriangulene Macrocycle on Au(111)

Kang Cui,[a] Florian Schlütter,[b] Oleksandr Ivasenko,[a] Milan Kivala,[b] Matthias G. Schwab, [b]‡ Shern-Long Lee,[a] Stijn F.L. Mertens, [a]# Kazukuni Tahara,[c] Yoshito Tobe,[c] Klaus Müllen,[b] Kunal S. Mali,* [a] Steven De Feyter*[a]

Abstract: We demonstrate multicomponent network formation using a shape persistent macrocycle (**MC6**) at the interface between an organic liquid and Au(111) surface. **MC6** serves as a versatile building block that can be co-adsorbed with a variety of organic molecules based on different types of non-covalent interactions at the liquid-solid interface. Scanning tunneling microscopy (STM) reveals formation of crystalline bicomponent networks upon co-deposition of **MC6** with aromatic molecules such as fullerene ($\mathbf{C_{60}}$) and coronene (**COR**). **TCNQ** on the other hand, was found to induce disorder into the **MC6** networks by adsorbing on the rim of the macrocycle. Immobilization of **MC6** itself was studied in two different non-covalently assembled host networks. **MC6** assumed a rather passive role as a guest and simply occupied the host cavities in case of one network whereas it induced a structural transition in the other. Finally, the central cavity of **MC6** was used to capture $\mathbf{C_{60}}$ in a complex three-component system. Precise immobilization of organic molecules at discrete locations within multicomponent networks as demonstrated here constitutes an important step towards bottom-up fabrication of functional surface-based nanostructures.

Introduction

One of the dominant themes in the research on two-dimensional (2D) molecular self-assembly has been the fabrication of crystalline supramolecular networks that consist of more than one component physisorbed on a solid surface.[1] An important objective within this research theme is the generation of solid interfaces with predictable nanoscale morphologies and properties. This trend is largely driven by potential applications in emerging fields such as molecular scale electronics, sensing and catalysis, which will benefit from the precise control over molecular organization on solid surfaces. Although real-life applications based on such interfaces are still at the *'proof-of-principle'* stage,[2] significant advances have already been made towards controlling the multicomponent molecular assembly on surfaces.[3] By careful selection of organic building blocks and via precise control over intermolecular as well as interfacial interactions, complex multicomponent surface architectures have been realized. The formation and structure of such interfaces via so called 2D crystallization processes can be studied at the molecular level under ultrahigh vacuum (UHV) conditions as well as at the liquid-solid interface using scanning tunneling microscopy (STM).[4]

A majority of 2D multicomponent self-assembled systems reported so far are based on host-guest interactions in which one component forms an ordered open network with well-defined voids. Such so called porous networks have garnered significant attention in the recent past since they can be used for immobilization of guest species such as single molecules or molecular clusters in spatially repetitive fashion, thus making the network functional.[5] Various host networks sustained by van der Waals[6], metal-ligand[7] or hydrogen bonding[8] interactions have been used to immobilize a variety of guest molecules. In several cases, guest molecules were found to induce structural changes into the self-assembling system such that a given type of network was only obtained in presence of the guest.[9] This templating ability of the guest species also highlights the dynamic nature of the multicomponent self-assembly. Alternatively, guest inclusion has also been accomplished by employing inherently porous building blocks such as shape persistent macrocycles.[10] However, non-covalently assembled porous networks often provide increased flexibility and versatility in building host-guest systems. A minority class of multicomponent networks is based on non-host-guest type systems where none of the components forms an open porous structure but the multicomponent network formation is driven by specific interactions between the assembling components which favor co-crystallization over phase separation.[11] A notable example is the four-component supramolecular architecture constructed by using shape complementarity of alkadiyne side chains, where well-ordered networks with repeat units as large as 23 nm were obtained.[11d]

Although the construction of self-assembled systems based on more than one type of molecules has been a subject

[a] K. Cui, Dr. O. Ivasenko, Dr. S.-L. Lee, Dr. S. F. L. Mertens, Dr. K. S. Mali, Prof. S. De Feyter
Division of Molecular Imaging and Photonics, Department of Chemistry, KU Leuven-University of Leuven, Celestijnenlaan 200F, 3001, Leuven, Belgium
#Vienna University of Technology, Institute of Applied Physics, 1040 Vienna, Austria.
Email: Kunal.Mali@chem.kuleuven.be
Email: Steven.DeFeyter@chem.kuleuven.be

[b] Dr. F. Schlütter, Dr. M. Kiwala, Dr. M. G. Schwab, Prof. K. Mullen
Max Planck Institute for Polymer Research, D-55128 Mainz, Germany. ‡ Present address: BASF SE, Carl-Bosch-Straße 38, 67056 Ludwigshafen, Germany.

[c] Dr. K. Tahara, Prof. Y. Tobe
Division of Frontier Materials Science, Graduate School of Engineering Science, Osaka University Toyonaka, Osaka 560-8531, Japan

Supporting information for this article is given via a link at the end of the document.

of intense scrutiny, crystalline networks that consist of three or more components are rare both at the UHV-solid[1d] and liquid-solid interface.[1a-c] This is mostly because the fabrication of such heteromeric structures requires efficient recognition between different molecular components and precise knowledge of intermolecular as well as molecule-substrate interactions. The liquid-solid interface adds further complexity to the multicomponent self-assembly since molecule-solvent and solvent-substrate interactions also need to be considered.[12] It has been observed that a stoichiometric ratio of molecules in solution that yields a crystalline multicomponent network is often different from what is anticipated from the structure of the targeted supramolecular network. This disparity occurs due to dissimilar adsorption energies of the different molecules involved in the process and thus arriving at a correct stoichiometric mole ratio in solution is often challenging.[1a] Given that recognition processes transpiring at the liquid-solid interface are fairly complex even for single component systems, avoiding phase separation of molecular components is a major challenge in such studies. Finally, self-assembly at the liquid-solid interface may or may not always take place under thermodynamic control and kinetic effects often play an important role in governing the outcome of the process.[13]

The nature of the substrate is also crucial, which essentially governs the mobility of molecules at the liquid-solid interface and thus the ability to 'self-repair'. While annealing the self-assembling system at higher temperatures can induce the necessary dynamics (often practiced under UHV conditions), the temperature window accessible for experiments carried out at the liquid-solid interface is often limited due to evaporative loss of the solvent. This especially becomes a serious concern for metal substrates such as Au(111), which tend to interact relatively strongly with aromatic molecules.[14] Controlling organization and achieving long range order via physisorption of molecules is thus often challenging on Au(111) as compared to highly oriented pyrolytic graphite (HOPG) due to higher diffusion barriers encountered in case of gold. As a consequence, HOPG has been the substrate of choice when studying multicomponent self-assembly under ambient conditions and more than two components have rarely been co-crystallized on Au(111).[14b] Thus, understanding of multicomponent self-assembly at the organic liquid/Au(111) interface is still in its infancy.

Here we explore the versatility of a π-conjugated organic macrocycle for the construction of two- and three-component self-assembled networks on Au(111). The building block central to the theme of this study is a so-called *N*-heterotriangulene macrocycle (**MC6,** Figure 1A) obtained by cyclisation of dimethylmethylene-bridged triphenylamines (DTPA).[15] It belongs to the class of shape-persistent polycyclic aromatic macrocycles, which have gained significant attention in the recent past due to their ability to form 1D columnar nanotubes, 2D porous networks and 3D inclusion complexes via self-assembly.[16] Upon appropriate functionalization, such triarylamines have also been used as hole-transport materials in organic light emitting diodes (OLEDs) and organic field effect transistors (OFETs).[17] Furthermore, the presence of nitrogen atoms in the backbone makes these macrocycles attractive candidates as molecular switches since they can undergo changes in charge and shape upon redox processes.[18]

In this paper, we report the construction of two- and three-component surface-confined composites based on **MC6** at the liquid-solid interface. Studying the adsorption and assembly of such high molecular weight compounds using STM is relatively straightforward at the liquid-solid interface than under UHV conditions due to the difficulty associated with their sublimation. We first show that **MC6** itself forms ordered 2D molecular network on a Au(111) surface which could be further used to host a variety of guest molecules such as fullerene (C_{60}), coronene (**COR**) and tetracyanoquinodimethane (**TCNQ**). Depending on the nature of their interaction with **MC6** and the substrate, the guest molecules were found to occupy different sites within the host network on Au(111). Using STM at the organic liquid-solid interface, we show that C_{60} and **COR** prefer to occupy the interstitial sites of the **MC6** network whereas **TCNQ** adsorbs on the rim of the macrocycle. Furthermore, we also illustrate the immobilization of **MC6** as a guest in two dissimilar, non-covalently assembled host networks. **MC6** behaves differently upon co-adsorption with each host network. In case of host network formed by a dodecyloxy substituted dehydrobenzo[12]annulene (**DBA-OC12,** Figure 5A) derivative,[6] **MC6** prefers to adsorb in the hexagonal cavities of the honeycomb network whereas for dodecyloxy substituted tris-triphenylene (**TTP,** Figure 6A) host network,[19] it induces a change in the structure of the host network upon co-adsorption. Finally, the **DBA-MC6** system could be further used as a template to capture C_{60} molecules in the cavity of **MC6**. The **DBA-MC6-C_{60}** three-component system is a unique type of host-guest system as it combines an intrinsically porous covalent molecule (**MC6**) with a non-covalently assembled porous supramolecular network (**DBA**). The site selectivity of different guest molecules as demonstrated here is crucial for forming functional superstructures for the recognition of appropriate guest molecules. Moreover the ability to immobilize electron donating (**MC6)** and electron accepting (**TCNQ**, C_{60}) molecules in a spatially ordered fashion is vital for the development of complex nanostructures relevant to organic photovoltaics.

Results and Discussion

Each **MC6** molecule is composed of six DTPA units linked together in a cyclic fashion (Figure 1A). Thus the rim of the macrocycle has a high density of methyl groups, which raise the aromatic backbone of the molecule slightly above the Au(111) substrate thereby possibly imparting some mobility to the **MC6** molecules after deposition. A direct manifestation of this mobility is reflected in **MC6** adsorption on Au(111) which results in ordered network formation despite the high molecular weight of the building block. Figure 1B provides a large scale STM image of **MC6** monolayer formed at the TCB/Au(111) interface in which the molecules are arranged in a hexagonal fashion. Each bright flower-like feature corresponds to a single **MC6** molecule. The monolayer often shows defects. Apart from ordered domains that extend few hundred square nanometers, isolated disordered patches of molecules are also visualized (Figure S1 in the SI).

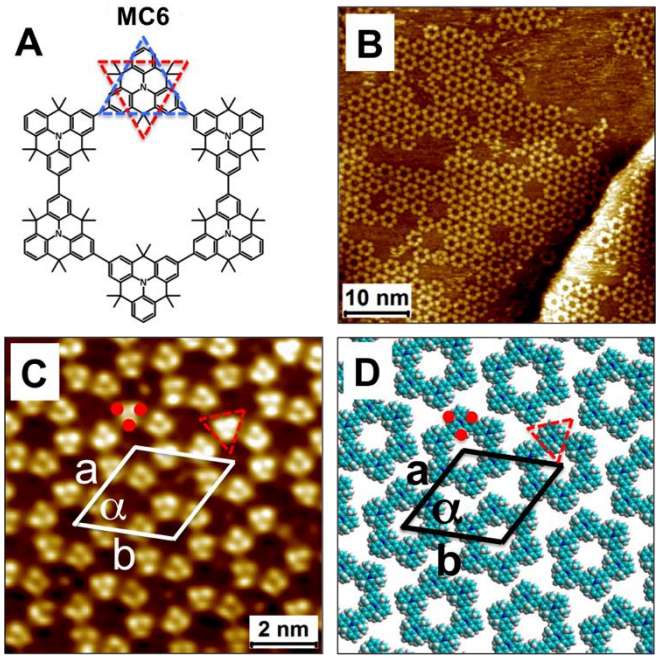

Figure 1. (A) Molecular structure of **MC6**. The blue triangle outlines the orientation of the aromatic part of the DTPA unit whereas the red triangle outlines the triangle formed by the methyl groups. (B) Large scale STM image of **MC6** adlayer formed at the TCB/Au(111) interface. [**MC6**] = 4.6 × 10^{-6} M (C) HR-STM image of **MC6** monolayer. Imaging conditions: V_{bias} = -200 mV, I_{set} = 80 pA. Unit cell contains one **MC6** molecule and the parameters are: $a = b$ = 3.0 ± 0.1 nm, α = 60.0 ± 2.0˚(D) A molecular model for the self-assembled structure. The red filled circles in (C) highlight the protrusions observed in each **MC6** subunit, which correspond to the methyl groups in the molecule as shown by corresponding filled circles in the molecular model (D).

Although single crystal X-ray analysis[15] had indicated an overall bent structure of the macrocycle owing to the steric demand of the bridging methyl groups, high-resolution STM (HR-STM) imaging did not reveal any obvious non-planarity in the molecular backbone of **MC6**. This could be a result of planarization of **MC6** upon adsorption onto the Au(111) surface.The HR-STM image provided in Figure 1C clearly reveals that each **MC6** molecule appears as a ring made up of six triangular sub-units. Each triangle corresponds to an individual DTPA unit and is made up of three bright protrusions. Comparison of the HR-STM image with the molecular structure (Figure 1A) and the model provided in Figure 1D further illustrates that these protrusions arise from the methyl groups (red filled circles) and not from the aromatic core of **MC6** (blue triangle in Figure 1A). The central cavity of **MC6** shows darker contrast relative to the rim of the macrocycle. The diameter of the cavity measured from STM images is 1.1 ± 0.1 nm, which is in good agreement with that obtained from single crystal X-ray analysis.[15] This space can be used for the immobilization of guest species. Apart from the central cavity of each molecule, the **MC6** network also offers empty spaces in the form of interstitial sites, which could also be used for guest inclusion. The area of an interstitial site is comparable to that offered by the intrinsic cavity of **MC6** (~1 nm^2).

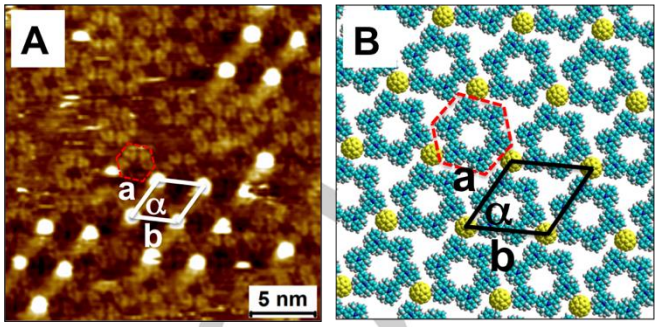

In the following, we describe bicomponent network formation using **MC6**.

Figure 2. (A) STM image of the bicomponent network formed upon co-adsorption of **MC6** and **C_{60}** at the TCB/Au(111) interface. [**MC6**] = 2.3 × 10^{-6} M, [**C_{60}**] = 1.4 × 10^{-7} M; Imaging conditions: V_{bias} = -200 mV, I_{set} = 60 pA. The unit cell contains one molecule of MC6 and C_{60} each and the cell parameters are a = 3.3 ± 0.1 nm; b = 3.3 ± 0.1 nm; α = 60.0 ± 2.0˚. The red hexagon highlights a single **MC6** molecule. (B) A molecular model for the self-assembled network.

C_{60} was selected as a guest based on its size (van der Waals diameter = 1.1 nm) and spherical shape, which is ideally suited for immobilization into the cavity of **MC6**. Co-adsorption of **MC6** and **C_{60}** was attempted using sequential deposition in which the adlayer of **MC6** was first formed at the TCB/Au(111) interface followed by addition of **C_{60}** from a TCB solution. Figure 2A shows STM image of the surface obtained upon such sequential deposition. The bright features correspond to **C_{60}** molecules. Upon a careful inspection, **MC6** molecules, which appear with lower apparent height, can also be seen in the STM image. Contrary to expectation, **C_{60}** adsorption occurred in the interstitial sites instead of the cavity of **MC6**. The unit cell of the **MC6/C_{60}** network is slightly larger than that for the **MC6** monolayer (Figure 1C) indicating that **C_{60}** adsorption in the interstices expands the host network. Comparison of the STM image with the molecular model provided in Figure 2B further clarifies the structure of the bicomponent network. A possible reason for the preferential interstitial adsorption of **C_{60}** could be stronger **C_{60}**-Au interactions, which prevent its capture by the **MC6** cavity where it would be stabilized only by weak van der Waals interactions (also see Figure S2 in SI). On the other hand, **C_{60}**-Au(111) interactions are relatively strong (40-60 kcal/mol)[22] and are dominated by charge transfer from the Au substrate to **C_{60}**. Adsorption in the interstitial sites thus stabilizes the **C_{60}** molecules not only via strong molecule-substrate interactions but also through van der Waals stabilization offered by the methyl groups of surrounding **MC6** molecules. Moreover, a peculiar aspect of C_{60} adsorption in the present case is that only one out of two possible interstitial sites are regularly occupied. One plausible explanation for such behavior could be charge transfer interactions between the host and guest, which render only every alternate site electrostatically suitable for adsorption of C_{60}. The fabrication of the two-component **MC6-C_{60}** system was severely limited by the narrow concentration range in which both the components could be observed on the surface. A slight increase in the concentration of

C_{60} often lead to its preferential adsorption thereby completely displacing **MC6** from the Au(111) surface (Figure S3 in SI).

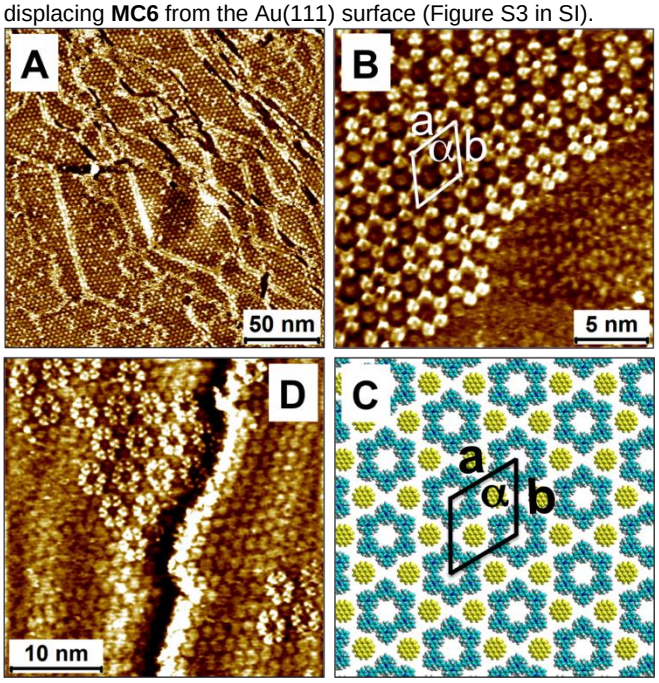

Figure 3. (A) Large-scale STM image of the **MC6/COR** bicomponent network formed at the TCB/Au(111) interface. [**MC6**] = 2.3 × 10^{-6} M, [**COR**] = 2.3 × 10^{-6} M; (B) Corresponding HR-STM image. The disc-like features in between **MC6** molecules are the co-adsorbed **COR** molecules. Imaging conditions: V_{bias} = -200 mV, I_{set} = 80 pA. The unit cell contains one molecule of **MC6** and two molecules of **COR** with: a = 3.5 ± 0.1 nm; b = 3.5 ± 0.1 nm; α = 59.0 ± 2.0˚. (C) A molecular model for the self-assembled network. (D) Surface architecture obtained upon using excess **COR**.

In contrast to the **MC6/C_{60}** system, the **MC6/COR** networks could be formed at variety of different concentrations and well-ordered bicomponent networks were observed. Deposition of **COR** on preformed monolayer of **MC6** furnished crystalline molecular networks, which extend over several hundred square nanometers. Figure 3A shows a large scaleSTM image of the **MC6/COR** network. The size of the domains obtained after deposition of **COR** is much larger than that observed for **MC6** adsorption alone. This clearly indicates that **COR** facilitates the adsorption of **MC6** into large defect-free domains. HR-STM image displayed in Figure 3B provides a clue to the templating behavior of **COR**. The interstitial sites are occupied by disk-like features which we ascribe to adsorption of **COR**. In such co-assembled structure, the **COR** molecules are expected to be stabilized by van der Waals interactions with the methyl groups of surrounding **MC6** molecules. Measurement of the unit cell parameters indicates that **COR** adsorption expands the **MC6** network and also changes the relative orientation of the **MC6** molecules with respect to each other (see Figure 1C for comparison). The lower right corner of the STM image shows a separate domain of bright features.

Based on the distance between these features (1.2 nm) obtained from self-correlation analysis, we conclude that this is a phase-separated domain of **COR**. Furthermore, a number of **MC6**

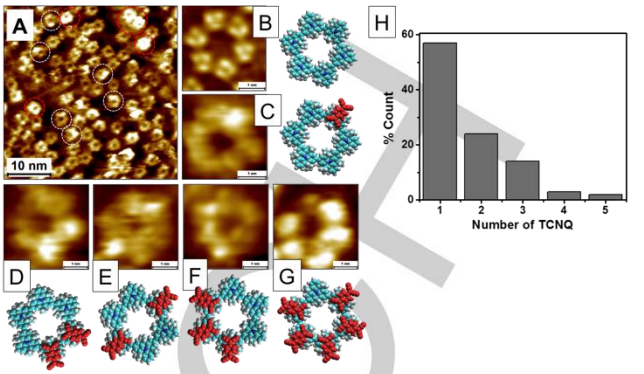

cavities appear bright indicating some adsorption in the cavity. Given that **COR** has larger π surface area in contact with

Figure 4. (A) STM image depicting the loss of order in the **MC6** monolayer upon deposition of **TCNQ** at the Au(111)/TCB interface. [**MC6**] = 1.6 × 10^{-6} M, [**TCNQ**] = 5 × 10^{-6} M. Imaging conditions: V_{bias} = -200 mV, I_{set} = 80 pA. **MC6** molecules exhibit varying contrast along the rim indicating charge-transfer complex formation with added **TCNQ**. Molecules that exhibit complete charge-transfer complex formation along the rim (presumably with six **TCNQ** molecules) are highlighted with red circles whereas white circles show those partially complexed. (B)-(F) Magnified **MC6** molecules showing varying degree of complexation together with tentative molecular models for each complex. **TCNQ** molecules are shown in red. (H) Histogram showing the number distribution of **TCNQ** molecules adsorbed per molecule of **MC6**.

the substrate compared to **C_{60}**, it is expected to have stronger interactions with Au(111). Thus, it is not unreasonable to assume that **COR** adsorption does not occur only in the interstitial sites but also possibly in the cavity of **MC6**, albeit **COR** adsorbs underneath the macrocycle due to its larger diameter than that of the cavity. Co-adsorption experiments carried out using excess **COR** revealed formation of a **COR** monolayer with small isolated patches of **MC6** as shown in Figure 3D. Analysis of these STM images based on the unit cell parameters of **COR** on Au(111)[14b] reveal that although there is a possibility of **COR** adsorption underneath the cavity of **MC6**, the **COR** monolayer is not continuous (see also Figure S4 in SI).

A third guest molecule, namely **TCNQ**, was chosen due to its strong electron deficient nature. **TCNQ** lacks the shape and size complementarity to perfectly fit into either the central cavity of **MC6** or in the interstitial sites, however owing to its electron deficient nature it is expected to interact with the electron rich backbone of **MC6**. Similar to the **MC6/C_{60}** system, a careful control over the relative ratio of the two components was crucial in order to observe both **MC6** and **TCNQ** on the surface. Deposition of **TCNQ** on **MC6** adlayer always led to loss of order in **MC6** monolayers. Figure 4A shows an STM image depicting the change in the monolayer of **MC6** upon addition of **TCNQ** to the surface. Apart from the disordered nature of the **MC6** monolayer, one can easily notice the unevenness of STM contrast along the **MC6** backbone. Some **MC6** molecules appear much brighter than others (red circles) whereas some of them show bright protrusions along the rim (white circles). These unusual contrast features are more apparent when one compares the appearance of a single **MC6** molecule in absence of **TCNQ**

(Figure 4B) with that in presence of **TCNQ** as shown in Figures 4C-4G. The bright features can thus be readily attributed to the adsorption of **TCNQ** molecules along the rim of **MC6**. Such adsorption is a result of donor-acceptor (D-A) complex formation between **TCNQ** and the electron rich DTPA units that constitute **MC6**. Assuming that each DTPA unit is involved in one D-A stack with **TCNQ**, in principle, every **MC6** molecule offers six positions where such complexation can occur. Figure 4A shows that complexation at multiple sites within a single **MC6** molecule is possible and occasionally all six sites were found to be occupied by **TCNQ** molecules (red circles in Figure 4A).

Statistical analysis of STM images of the **MC6/TCNQ** network revealed that although all six DTPA units within a single **MC6** molecule are equivalent, the binding ability of the **MC6** molecule as a whole decreases upon interaction with subsequent **TCNQ** molecules. The histogram displayed in Figure 4H provides the number distribution of **TCNQ** molecules adsorbed per **MC6** molecule and clearly illustrates that a large number of **MC6** molecules prefer to complex with fewer number of guests. This is possibly a result of relatively weaker electron-donating ability of the already formed **MC6/TCNQ** complex relative to **MC6** itself. The changes in the electronic structure of **MC6** molecules upon complexing with **TCNQ** could be further invoked to explain the loss of long-range order in the **MC6** monolayer observed upon addition of **TCNQ**. It has been well established by now that 2D crystal formation is a result of delicate balance between intermolecular and interfacial interactions. Any imbalance caused by the charge transfer or charge redistribution at the molecule/substrate interface can affect network formation.[23] It can be readily understood that upon complexing with one or more **TCNQ** molecules, the originally symmetric electron density of **MC6** will be affected, resulting in an intrinsic dipole in the macrocycle. The ensuing repulsive interactions between differently complexed **MC6/TCNQ** composites thus destroy the long-range order typically observed within domains. Additionally, the disorder may also arise from the loss of original C6-symmetry of the MC6 molecules (due to random complexation) and reduction in optimal van der Waals contact between **MC6** molecules due to **TCNQ** adsorption on the rim of the macrocycle. Lastly, competitive adsorption of **TCNQ** molecules directly on Au(111) also needs to be considered for explaining the observed disorder in the two-component network.

Having explored the ability of **MC6** to form bicomponent networks with different guest molecules, we now discuss fabrication of bicomponent systems in which **MC6** acts as an intrinsically porous guest. For immobilization of **MC6**, two different building blocks, namely **DBA**[6] and **TTP**[19], which are known to form porous host networks based on van der Waals interactions, were used. The choice of these host networks was based on the size and shape of the hexagonal cavities, which are well suited to capture **MC6**.

Alkoxy substituted **DBA** derivatives form honeycomb networks based on interdigitation of alkoxy chains.[6] The van der Waals interaction between the chains is the main driving force for the formation and stabilization of these porous networks. **DBA-OC$_{12}$** forms a porous network upon adsorption at the Au(111)/TCB

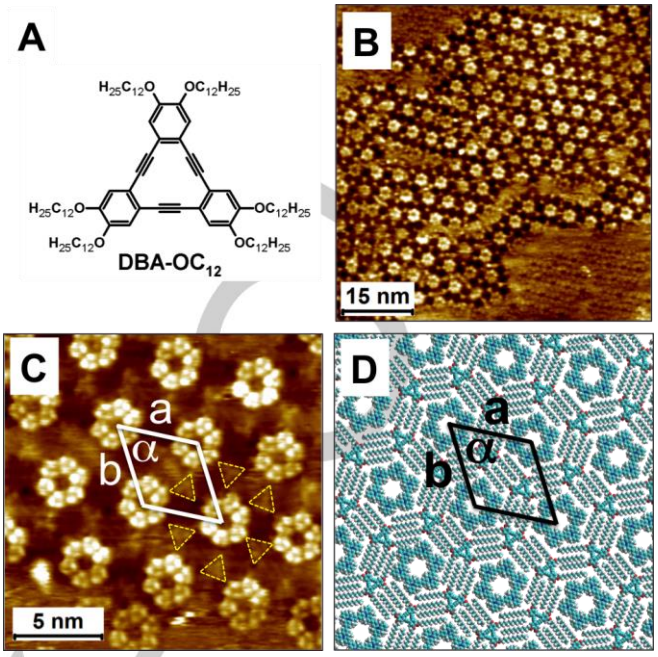

Figure 5. (A) Molecular structure of **DBA-OC$_{12}$**. (B) Large-scale STM image of the **DBA-OC$_{12}$/MC6** bicomponent network formed at the TCB/Au(111) interface. **[DBA-OC$_{12}$]** = 4.0 × 10^{-7} M, **[MC6]** = 1.6 × 10^{-6} M. Apart from the co-crystallized domain in which **MC6** occupies the hexagonal cavity of the honeycomb network, small **MC6** domains are also visible in the upper left and lower right corner of the image. (C) Corresponding HR-STM image. **DBA-OC$_{12}$** molecules, which exhibit low apparent height than **MC6**, are marked with yellow triangles. Imaging conditions for (B) as well as (C): V_{bias} = -200 mV, I_{set} = 80 pA. The unit cell contains two molecules of **MC6** and one molecule of **DBA-OC$_{12}$** with: a = 4.6 ± 0.2 nm; b = 4.7 ± 0.3 nm; α = 60.0 ± 2.0°. (B) A molecular model depicting the self-assembled network.

(Figure S5 in SI). **DBA-OC$_{12}$/MC6** bicomponent system was obtained by deposition of a premixed solution **[1 (DBA-OC12): 4 (MC6)]** containing the two components in TCB. Figure 5B shows a large scale STM image of the host-guest network. Besides the co-crystallized domains where **MC6** occupies the hexagonal cavity of the **DBA-OC$_{12}$** network, small phase-separated domains of **MC6** were also found as seen in the lower right and upper left corner of the STM image. The relative ratio of the two components is crucial for realization of a long-range ordered host-guest network. As previously known for the DBA derivatives[24], relatively higher concentrations of **DBA-OC$_{12}$** lead to formation of a high-density linear polymorph (Figure S6 in SI) which cannot accommodate **MC6** due to lack of open structure whereas lowering the relative concentration of **DBA-OC$_{12}$** lead to formation of crystalline host-guest networks which co-existed with small domains of **MC6**. Reducing the relative concentration of **MC6** lead to formation of a binary network in which a number of DBA hexagons remained empty (Figure S7 in SI). Figure 5C shows a HR-STM image of the **DBA-OC$_{12}$/MC6** network. The host network is feebly visible due to the higher apparent height of the **MC6** molecules. However, triangular **DBA-OC$_{12}$** molecules (yellow

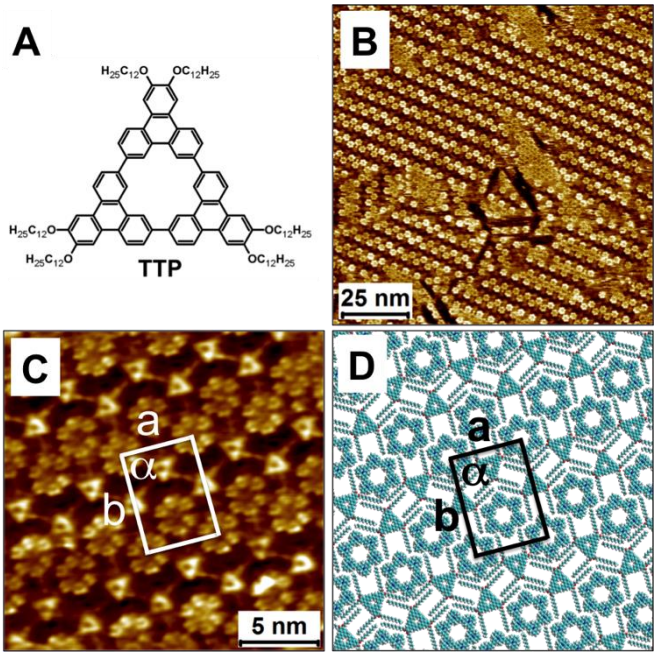

triangles) can be discerned upon careful observation. **MC6** acts as a typical guest and its incorporation into the host

Figure 6: (A) Molecular structure of **TTP**. (B) Large-scale STM of the **TTP/MC6** bicomponent network formed at the TCB/Au(111) interface. [**TTP**] = 2.8×10^{-7} M [**MC6**] = 2.3×10^{-6} M **[1 (TTP): 4 (MC6)]**. (C) HR-STM images of the **TTP/MC6** network. The rectangular unit cell contains two molecules of **MC6** and **TTP** each with: a = 4.9 ± 0.2 nm; b = 6.7 ± 0.2 nm; α = 89.0 ± 3.0˚. Imaging conditions for (B) as well as (C) are: V_{bias} = -200 mV, I_{set} = 100 pA (D) Molecular model for the self-assembled network.

network does not induce any structural transition as previously reported for other host networks.[9]

Comparison of the **DBA/MC6** system with a three-component network involving a slightly different DBA derivative reported recently merits a special attention here. This system consisted of a **DBA-OC$_{10}$** network that hosts a heterocluster formed by six molecules of isophthalic acid (ISA) and a molecule of **COR** at the 1-octanoic acid/Au(111) interface.[14b] The guest cluster was found to induce formation of a superlattice structure involving chiral and achiral pores within the host network. The superlattice formation was explained on the basis of initial nucleation of the guest cluster, which favors the formation of an achiral pore. Geometric requirements imposed by accommodation of additional guest clusters then resulted in the formation of an ordered superlattice. For the **DBA-OC$_{12}$/MC6** system however, we did not detect any such phenomenon. The lack of any superlattice formation in the present case relates to the fundamental difference in the nature of **MC6** compared to the COR-ISA guest clusters. One readily expects that the templating ability of **MC6** is much weaker than a COR-ISA cluster in view of reduced molecule-substrate interactions for the former. Thus, **MC6** acts as a rather passive guest that only fills up the host cavities.

Dodecyloxy substituted **TTP**[21] (Figure 6A) is similar to **DBA-OC$_{12}$** in terms of its symmetry, however the aromatic core

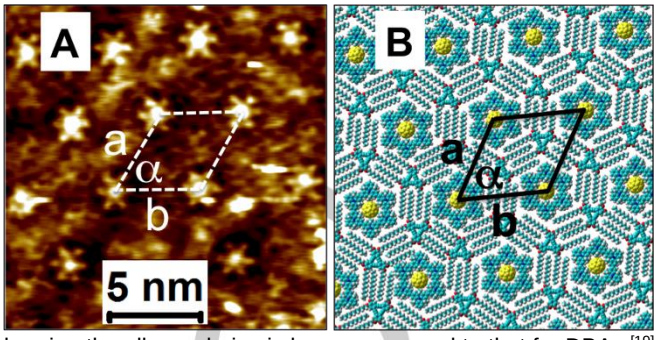

bearing the alkoxy chains is larger compared to that for DBAs.[19] Similar to **DBA-OC$_{12}$**, **TTP** self-assembly also furnished porous

Figure 7: (A) STM images showing the formation of three component **DBA-OC$_{12}$/MC6/C$_{60}$** system at the TCB/Au(111) interface. [**DBA-OC$_{12}$**] = 4.0×10^{-7} M, [**MC6**] = 1.6×10^{-6} M, [**C$_{60}$**] = 8.0×10^{-7} M. **DBA-OC$_{12}$** molecules are not visualized in the STM image. The unit cell contains two molecules of **DBA-OC$_{12}$** and one molecule of **MC6** and **C$_{60}$** each with: a = 4.8 ± 0.3 nm; b = 5.0 ± 0.3 nm; α = 60.0 ± 3.0˚. Imaging conditions: V_{bias} = -200 mV, I_{set} = 80 pA (B) Molecular model for the self-assembled system.

networks however with exclusive surface coverage of distorted hexagonal pores (Figure S9 in SI). A larger number of distorted pores indicate that the self-assembly is driven by kinetic effects which are plausibly governed by the strong interaction between the aromatic core of **TTP** and Au(111).

Deposition of a premixed solution of **TTP** and **MC6 [1 (TTP): 4 (MC6)]** on Au(111) surface gave rise to an entirely new supramolecular pattern (Figure 6B) in which **MC6** molecules are arranged in a zigzag fashion. The domains are typically large and extend over several hundred square nanometers. Patches of phase-separated **MC6** coexist with the co-crystallized domains. HR-STM image provided in Figure 6C clearly reveals the formation of a bicomponent network. The bright triangles with a depression in the center are the aromatic cores of **TTP** molecules and they follow the same zigzag pattern as that of **MC6**. A molecular model based on the STM image (Figure 6D) reveals that only four out of six dodecyloxy chains are involved in interdigitation with neighboring **TTP** molecules. The other two chains could be simply adsorbed on the surface without any interdigitation or be solvated in the supernatant.

At this juncture it is essential to discuss the different outcome of the co-assembly experiments of **MC6** with **DBA-OC$_{12}$** and **TTP**. While the 2D network of **DBA** was preserved upon co-adsorption with **MC6**, the rather disordered network of **TTP** underwent a structural transition. This difference is a good illustration of how the competition between **DBA**-**DBA**, **DBA**-**MC6**, **TTP**-**TTP**, **TTP**-**MC6** and **MC6**-**MC6** interactions affects the overall assembly process. It must be noted that the alkoxy chain separation on the DBA core is ideal for efficient interdigitation thereby maximizing the van der Waals interactions between the chains.[20, 25] Any possible stabilizing contribution of **MC6** is energetically no match for the inherent stabilization of the alkoxy chains in **DBA** networks. This leaves **MC6** with a secondary role, too weak to provide any templating effect as discussed earlier. The **TTP** network, on the other hand, has much smaller

stabilization from the interdigitation of the chains. This is primarily due to larger inter-chain separation on the **TTP**[19] core but also due to the stronger interactions between the aromatic core and the Au substrate. As a result, **MC6** is capable of templating **TTP** self-assembly into a network where the alkoxy chains are stabilized not only via relatively more efficient interdigitation but also through van der Waals interactions with **MC6**. Furthermore, it must be noted that while the distorted pores of **DBA-OC$_{12}$** are still capable of immobilizing **MC6**, this is not possible for the distorted pores of **TTP** as the distortion reduces the size of the pore significantly due to its larger core size (Figures S8 and S9 in SI).

Finally, we explored the possibility of guest incorporation in the cavity of **MC6** that is already immobilized in a **DBA-OC$_{12}$** host network. **C$_{60}$** was selected as a guest due to its better fit in the cavity of **MC6** and also keeping in mind the possible future applications of **MC6/C$_{60}$** composites due to the attractive electronic properties of the two molecules. Contemplating the results on the **MC6/C$_{60}$** system described earlier, we reasoned that if the Au(111) surface is already masked by the **MC6/DBA-OC$_{12}$** network, **C$_{60}$** should be immobilized into the **MC6** cavity instead of directly adsorbing on the substrate. Figure 7A shows an STM image of the surface obtained after deposition of TCB solution of **C$_{60}$** on a preformed **MC6/DBA-OC$_{12}$** network. Features reminiscent of the bicomponent network can be clearly identified in the STM image, however a major difference is the appearance of the **MC6** cavities. In contrast to the **MC6/DBA-OC$_{12}$** networks, the cavities appear bright indicating adsorption of **C$_{60}$** (also see Figure S10 in SI). The bright protrusion seen in the STM image is around 1.1 nm in diameter further corroborating the immobilization of **C$_{60}$**. Although the **DBA-OC$_{12}$** molecules could not be visualized in the three-component system, their presence is confirmed by the unit cell parameters, which are identical to that obtained for **DBA-OC$_{12}$-MC6** system. To our knowledge this is one of only a few examples[14b] of a three component crystalline network obtained on a Au(111) substrate.

Conclusions

Controlling nanoscale structure of organic adlayers is crucial for various applications because spatial arrangement of building blocks often affects the function of the layer. Multicomponent adlayers further add to the versatility in terms of both structure as well as function. Regulating the structure of physisorbed self-assembled monolayers made up of more than one type of molecule thus constitutes an important yet challenging task. In this study we have demonstrated multicomponent network formation using a functional shape persistent macrocycle exercising the principles of 2D crystal engineering. Crystalline supramolecular networks of varying complexity were constructed successfully at the liquid-solid interface. **MC6** served as a docking station for different guests via a multitude of different supramolecular interactions. Furthermore, a unique three component system based on host-guest interactions was realized in which a porous molecule was immobilized as a guest in a supramolecularly assembled porous host network. The covalent guest then served as a host to capture a **C$_{60}$** molecule. Identification of such versatile building blocks as **MC6** is crucial for utilizing a variety of different supramolecular interactions for building complex functional materials based on organic building blocks.

Experimental Section

All experiments were performed at room temperature (20-24 ℃) using a PicoLE (Agilent) system operating in constant-current mode with the tip immersed in the supernatant liquid. STM tips were prepared by mechanical cutting of Pt/Ir wire (80%/20%, 0.25 mm). Au(111) films on mica (Georg Albert PVD) were used as substrates. The substrates were annealed in a butane flame followed by cooling under a stream of argon. Reconstruction lines of Au(111) were not always present after sample annealing. 1,2,4-Trichlorobenezene (TCB, Sigma-Aldrich, 99%) was used as a solvent without further purification. For each measurement a 8 µL drop of the desired solution was applied directly to the flame annealed substrate and STM imaging commenced immediately. Syntheses of **MC6** [15], **DBA-OC$_{12}$**[20] and **TTP**[21] are reported elsewhere. **COR** (Sigma-Aldrich, 99%), **C$_{60}$** (Sigma-Aldrich, 99%), **TCNQ** (Sigma-Aldrich, 99%) were used without further purification. STM images were analysed using SPIP (Image Metrology, version 5.1.4) software and the molecular models were built using Hyperchem 7.0 program.

Acknowledgements

K.C. acknowledges receipt of a PhD scholarship from the China Scholarship Council, S.F.L.M. the receipt of a Marie Curie European reintegration grant, and O. I. thanks the Fund of Scientific Research—Flanders (FWO) for postdoctoral fellowship. This work was further supported by the Belgian Federal Science Policy Office via the IAP-PAI network “Functional Supramolecular Systems” (IAP 7/05), KU Leuven via GOA 11/003, FWO, advanced ERC grant Oxide Surfaces, and Grant-in-Aid for Scientific Research from the Ministry of Education, Culture, Sports, Science, and Technology, Japan. This research also received support from the European Research Council under the European Union’s Seventh Framework Programme (FP7/2007-2013)/ERC Grant Agreement no. 340324.

Keywords: host-guest system • Au(111) • STM • self-assembly • shape persistent macrocycle

[1] a) J. Adisoejoso, K. Tahara, S. Okuhata, S. Lei, Y. Tobe and S. De Feyter, *Angew. Chem. Int. Ed.* 2009, *48*, 7353-7357; b) J. Liu, T. Chen, X. Deng, D. Wang, J. Pei and L.-J. Wan, *J. Am. Chem. Soc.* 2011, *133*, 21010-21015; c) S. Lei, M. Surin, K. Tahara, J. Adisoejoso, R. Lazzaroni, Y. Tobe and S. D. Feyter, *Nano Lett.* 2008, *8*, 2541-2546; d) J. A. Theobald, N. S. Oxtoby, M. A. Phillips, N. R. Champness and P. H. Beton, *Nature* 2003, *424*, 1029-1031; e) M. Li, K. Deng, S.-B. Lei, Y.-L. Yang, T.-S. Wang, Y.-T. Shen, C.-R. Wang, Q.-D. Zeng and C. Wang, *Angew. Chem. Int. Ed.* 2008, *47*, 6717-6721; f) M. Surin and P. Samorì, *Small* 2007, *3*, 190-194; g) S. J. H. Griessl, M. Lackinger, F. Jamitzky, T. Markert, M. Hietschold and W. M. Heckl, *Langmuir* 2004, *20*, 9403-9407; h) S. J. H. Griessl, M. Lackinger, F. Jamitzky, T. Markert, M. Hietschold and W. M. Heckl, *J. Phys. Chem. B* 2004, *108*, 11556-11560; i) M. O. Blunt, J. C. Russell, C. Gimenez-LopezMaria del, N. Taleb, X. Lin, M. Schröder, N.

R. Champness and P. H. Beton, *Nat Chem* 2011, *3*, 74-78; j) O. Ivasenko, J. M. MacLeod, K. Y. Chernichenko, E. S. Balenkova, R. V. Shpanchenko, V. G. Nenajdenko, F. Rosei and D. F. Perepichka, *Chem. Commun.* 2009, 1192-1194; k) L. Piot, F. Silly, L. Tortech, Y. Nicolas, P. Blanchard, J. Roncali and D. Fichou, *J. Am. Chem. Soc.* 2009, *131*, 12864-12865; l) Y. Wakayama, D. G. de Oteyza, J. M. Garcia-Lastra and D. J. Mowbray, *ACS Nano* 2010, *5*, 581-589.

[2] a) B. Hulsken, R. Van Hameren, J. W. Gerritsen, T. Khoury, P. Thordarson, M. J. Crossley, A. E. Rowan, R. J. M. Nolte, J. A. A. W. Elemans and S. Speller, *Nat Nanotechnol* **2007**, *2*, 285-289; b) A. Ciesielski, S. Lena, S. Masiero, G. P. Spada and P. Samorì, *Angew. Chem. Int. Ed.* **2010**, *49*, 1963-1966; c) H. Xu, W. J. Saletra, P. Iavicoli, B. Van Averbeke, E. Ghijsens, K. S. Mali, A. P. H. J. Schenning, D. Beljonne, R. Lazzaroni, D. B. Amabilino and S. De Feyter, *Angew. Chem. Int. Ed.* **2012**, *51*, 11981-11985; d) T. Kudernac, N. Ruangsupapichat, M. Parschau, B. Macia, N. Katsonis, S. R. Harutyunyan, K.-H. Ernst and B. L. Feringa, *Nature* **2011**, *479*, 208-211.

[3] A. Ciesielski, C.-A. Palma, M. Bonini and P. Samorì, *Adv. Mater.* **2010**, *22*, 3506-3520.

[4] a) J. V. Barth, *Annu Rev Phys Chem* **2007**, *58*, 375-407; b) J. A. A. W. Elemans, S. Lei and S. De Feyter, *Angew. Chem. Int. Ed.* **2009**, *48*, 7298-7332; c) S.-S. Li, B. H. Northrop, Q.-H. Yuan, L.-J. Wan and P. J. Stang, *Acc. Chem. Res.* **2008**, *42*, 249-259; d) Y. Yang and C. Wang, *Chem. Soc. Rev.* **2009**, *38*, 2576-2589.

[5] T. Kudernac, S. Lei, J. A. A. W. Elemans and S. De Feyter, *Chem. Soc. Rev.* **2009**, *38*, 402-421.

[6] K. Tahara, S. Lei, J. Adisoejoso, S. De Feyter and Y. Tobe, *Chem. Commun.* **2010**, *46*, 8507-8525.

[7] a) S. Stepanow, M. Lingenfelder, A. Dmitriev, H. Spillmann, E. Delvigne, N. Lin, X. Deng, C. Cai, J. V. Barth and K. Kern, *Nat Mater* **2004**, *3*, 229-233; b) A. Langner, S. L. Tait, N. Lin, C. Rajadurai, M. Ruben and K. Kern, *Proc. Nat. Acad. Sci.* **2007**, *104*, 17927-17930.

[8] X. Zhang, Q. Zeng and C. Wang, *RSC Advances* **2013**, *3*, 11351-11366.

[9] a) S. Furukawa, K. Tahara, F. C. De Schryver, M. Van der Auweraer, Y. Tobe and S. De Feyter, *Angew. Chem. Int. Ed.* **2007**, *46*, 2831-2834; b) M. Blunt, X. Lin, M. d. C. Gimenez-Lopez, M. Schroder, N. R. Champness and P. H. Beton, *Chem. Commun.* **2008**, 2304-2306; c) D. Wu, K. Deng, M. He, Q. Zeng and C. Wang, *Chemphyschem* **2007**, *8*, 1519-1523; d) M. Li, P. Xie, K. Deng, Y.-L. Yang, S.-B. Lei, Z.-Q. Wei, Q.-D. Zeng and C. Wang, *Phys. Chem. Chem. Phys.* **2014**, *16*, 8778-8782; e) D. Bléger, D. Kreher, F. Mathevet, A.-J. Attias, G. Schull, A. Huard, L. Douillard, C. Fiorini-Debuischert and F. Charra, *Angew. Chem. Int. Ed.* **2007**, *46*, 7404-7407.

[10] a) B. Schmaltz, A. Rouhanipour, H. J. Räder, W. Pisula and K. Müllen, *Angewandte Chemie* **2009**, *121*, 734-738; b) G.-B. Pan, X.-H. Cheng, S. Höger and W. Freyland, *J. Am. Chem. Soc.* **2006**, *128*, 4218-4219; c) W. Huang, T.-Y. Zhao, M.-W. Wen, Z.-Y. Yang, W. Xu, Y.-P. Yi, L.-P. Xu, Z.-X. Wang and Z.-J. Gu, *J. Phys. Chem. C* **2014**, *118*, 6767-6772; d) K. Tahara, S. Lei, W. Mamdouh, Y. Yamaguchi, T. Ichikawa, H. Uji-i, M. Sonoda, K. Hirose, F. C. De Schryver, S. De Feyter and Y. Tobe, *J. Am. Chem. Soc.* **2008**, *130*, 6666-6667.

[11] a) Y. Xue and M. B. Zimmt, *Chem. Commun.* **2011**, *47*, 8832-8834; b) K. E. Plass, K. M. Engle, K. A. Cychosz and A. J. Matzger, *Nano Lett.* **2006**, *6*, 1178-1183; c) K. S. Mali, B. Van Averbeke, T. Bhinde, A. Y. Brewer, T. Arnold, R. Lazzaroni, S. M. Clarke and S. De Feyter, *ACS Nano.* **2011**, *5*, 9122-9137; d) Y. Xue and M. B. Zimmt, *J. Am. Chem. Soc.* **2012**, *134*, 4513-4516.

[12] S. De Feyter and F. C. De Schryver, *J. Phys. Chem. B* **2005**, *109*, 4290-4302.

[13] R. Gutzler, L. Cardenas and F. Rosei, *Chem. Sci.* **2011**, *2*, 2290-2300.

[14] a) A. Bhattarai, U. Mazur and K. W. Hipps, *J. Am. Chem. Soc.* **2014**, *136*, 2142-2148; b) T. Balandina, K. Tahara, N. Sändig, M. O. Blunt, J. Adisoejoso, S. Lei, F. Zerbetto, Y. Tobe and S. De Feyter, *ACS Nano* **2012**, *6*, 8381-8389.

[15] F. Schlütter, F. Rossel, M. Kivala, V. Enkelmann, J.-P. Gisselbrecht, P. Ruffieux, R. Fasel and K. Müllen, *J. Am. Chem. Soc.* **2013**, *135*, 4550-4557.

[16] a) M. Iyoda, J. Yamakawa and M. J. Rahman, *Angew. Chem. Int. Ed.* **2011**, *50*, 10522-10553; b) S. Höger, *Chem. Eur. J.* **2004**, *10*, 1320-1329.

[17] Y. Shirota and H. Kageyama, *Chem. Rev.* **2007**, *107*, 953-1010.

[18] A. Ito, Y. Yokoyama, R. Aihara, K. Fukui, S. Eguchi, K. Shizu, T. Sato and K. Tanaka, *Angew. Chem. Int. Ed.* **2010**, *49*, 8205-8208.

[19] K. S. Mali, M. G. Schwab, X. Feng, K. Mullen and S. De Feyter, *Phys. Chem. Chem. Phys.* **2013**, *15*, 12495-12503.

[20] K. Tahara, C. A. Johnson, T. Fujita, M. Sonoda, F. C. De Schryver, S. De Feyter, M. M. Haley and Y. Tobe, *Langmuir* **2007**, *23*, 10190-10197.

[21] M. G. Schwab, T. Qin, W. Pisula, A. Mavrinskiy, X. Feng, M. Baumgarten, H. Kim, F. Laquai, S. Schuh, R. Trattnig, E. J. W. List and K. Müllen, *Chem. Asian J.* **2011**, *6*, 3001-3010.

[22] Á. J. Pérez-Jiménez, J. J. Palacios, E. Louis, E. SanFabián and J. A. Vergés, *Chemphyschem* **2003**, *4*, 388-392.

[23] a) O. P. H. Vaughan, A. Alavi, F. J. Williams and R. M. Lambert, *Angew. Chem. Int. Ed.* **2008**, *47*, 2422-2426; b) T. Kudernac, N. Sändig, T. Fernández Landaluce, B. J. van Wees, P. Rudolf, N. Katsonis, F. Zerbetto and B. L. Feringa, *J. Am. Chem. Soc.* **2009**, *131*, 15655-15659.

[24] S. Lei, K. Tahara, F. C. De Schryver, M. Van der Auweraer, Y. Tobe and S. De Feyter, *Angew. Chem. Int. Ed.* **2008**, *47*, 2964-2968.

[25] E. Ghijsens, O. Ivasenko, K. Tahara, H. Yamaga, S. Itano, T. Balandina, Y. Tobe and S. De Feyter, *ACS Nano* **2013**, *7*, 8031-8042.

Entry for the Table of Contents

FULL PAPER

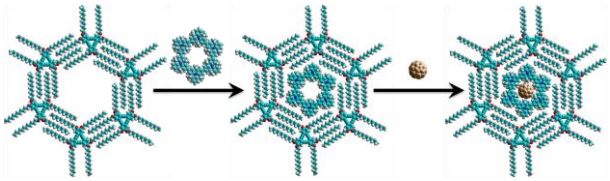

Multicomponent supramolecular network formation on Au(111) surface is demonstrated. We explore the versatility of a shape persistent aromatic macrocyle in forming complex noncovalent architectures at the organic liquid/solid interface. The macrocycle can act as a host or as a guest depening on the nature of the coadsorbing molecule. A hybrid system consisting of covalent as well as non-covalent hosts was realized when the macrocycle adsorbed in the cavity of a noncovalent host network was used to capture C_{60} in spatially repetitive fashion. The organic liquid/solid interface provides an ideal platform for studying such complex systems comprising high molecular weight compounds.

Kang Cui, Florian Schlütter, Oleksandr Ivasenko, Milan Kivala, Matthias G. Schwab, Shern-Long Lee, Stijn F.L. Mertens, Kazukuni Tahara, Yoshito Tobe, Klaus Müllen, Kunal S. Mali, Steven De Feyter**

Page No. – Page No.

Multicomponent Self-Assembly with a Shape Persistent *N*-Heterotriangulene Macrocycle on Au(111)